Single Molecule DNA Origami Nanoarrays with Controlled Protein Orientation

K. Cervantes-Salguero[1], M. Freeley[1], R. E. A. Gwyther[2], D. D. Jones[2], J. L. Chávez[3,*], M. Palma[1,*]

[1] Department of Chemistry, School of Physical and Chemical Sciences, Queen Mary University of London, London, United Kingdom
[2] Division of Molecular Biosciences, School of Biosciences, Main Building, Cardiff University, Cardiff, Wales, United Kingdom
[3] Air Force Research Laboratory, 711th Human Performance Wing, Wright Patterson Air Force Base, Dayton, Ohio, United States

For consideration by Biophysics Reviews- AIP

***Corresponding authors:**
jorge.chavez_benavides.2@us.af.mil; m.palma@qmul.ac.uk

Abstract

The nanoscale organization of functional (bio)molecules on solid substrates with nanoscale spatial resolution and single-molecule control – in both position and orientation- is of great interest for the development of next-generation (bio)molecular devices and assays. Herein, we report the fabrication of nanoarrays of individual proteins (and dyes) via the selective organization of DNA origami on nanopatterned surfaces, and with controlled protein orientation. Nanoapertures in metal-coated glass substrates were patterned using focused ion beam lithography; 88% of the nanoapertures allowed immobilization of functionalized DNA origami structures. Photobleaching experiments of dye-functionalized DNA nanostrucutres indicated that 85% of the nanoapertures contain a single origami unit, with only 3% exhibiting double occupancy. Using a reprogrammed genetic code to engineer into a protein new chemistry to allow residue-specific linkage to an addressable ssDNA unit, we assembled orientation-controlled proteins functionalized to DNA origami structures; these were then organized in the arrays and exhibited single molecule traces. This strategy is of general applicability for the investigation of biomolecular events with single-molecule resolution in defined nanoarrays configurations, and with orientational control of the (bio)molecule of interest.

I. INTRODUCTION

Nanoscale engineering of biomolecular arrays can facilitate the fabrication of next-generation (bio)molecular devices and assays.[1] In this regard, the organization of functional biomolecules on solid substrates with nanoscale spatial resolution with control at the level of individual molecules is of fundamental importance in order to develop biomimetic platforms capable of high-throughput single-molecule investigations.[2,3] Nanoscale biochips with such capabilities can surpass the current limits and would permit the monitoring of biochemical processes in real time, characterization of transient intermediates, and measurement of the distributions of molecular properties rather than their ensemble averages.[4] In particular, the precise placement of proteins within a nanoarray is of importance for the fabrication of biomimetic surfaces to be employed in cell adhesion and

spreading[5–7] investigations, drug discovery[8], as well as photobiophysical[9] and biosensing[10–12] applications.

Different techniques have been employed for fabricating biomolecular nanoarrays, including electron-beam,[3,13,14] Focused-Ion-Beam,[15] nanoimprint[16] and colloidal lithography,[17,18] thermochemical scanning probe lithography,[19] dip-pen,[20] photo-lithography,[21] PDMS imprint,[22] ink-jet microdeposition,[23] polymer brushes,[7,24] particle self-assembly[25–27] and bottom-up DNA origami[5,6,8,27–38]. These have opened new avenues for the development of high-throughput biosensing as well as for fundamental investigations of molecular interactions, including the protein-DNA interactions[39,40].

Among the different approaches for molecular organization, the use of DNA origami has shown to be an excellent bottom-up strategy due to high yielding self-assembled product in a single pot reaction, and addressable sites for facile and precise functionalisation with less than 6 nm (out of plane) resolution[30,41,42] subnanometer intermolecular distances[43,44] Moreover, spatial orientation control of single dyes was achieved using DNA origami[38]. Consequently, DNA origami has been utilized as nano-breadboards where molecular components such as proteins can be placed with single molecule control and organized into target configurations.[29,31,36,45–50] In particular, Marth et al. have shown positional control of proteins on a DNA origami, as well as orientational control via residue-specific incorporation of useful bioorthogonal reaction handles using a reprogrammed genetic code[28]. Based on the combination of both bottom-up DNA origami and top-down strategies, a photolithography strategy for producing fluorescent nanoarrays for photonics was devised[32]. More recently, a nanoarray strategy entirely relying on bottom-up self-assembly of microparticles and DNA origami was demonstrated and applied for super resolution studies[27]. Furthermore, our group demonstrated the fabrication, via a one-step lithographic process, of DNA origami nanoarrays[33] to investigate the role of biomimetic surfaces in cancer cell spreading[6].

Here, we present the fabrication of single protein nanoarrays via selective assembly of protein-DNA origami hybrids, arranged on nanopatterned surfaces, with control over the orientation of the protein tethered to the DNA nanostructures. The lattice-like nanoarrays were patterned on a metal-coated substrate via a single lithographic step using focused-ion beam milling (FIB)[51]. Green fluorescent protein (GFP), was modified at a specific residue with an oligonucleotide via a strain-promoted azide-alkyne coupling (SPAAC),[28,52,53] which was then hybridized to a complementary sequence at a specific position on the DNA origami. The DNA nanostructures were subsequently size-selected and selectively immobilized at the bottom of the nanoapertures of the aforementioned nanoarrays, via a biotin-streptavidin linkage strategy on silanized glass. Our strategy presents a facile method for immobilizing single proteins in a nanoarray with orientational control, and is of general applicability for the investigation, via fluorescence imaging, of biomolecular events with single-molecule resolution.

II. METHODS

Materials: All oligonucleotides and modified oligonucleotides were purchased from Integrated DNA Technologies (IDT). M13mp18 viral DNA was purchased from Tilibit. Streptavidin, Dulbecco's phosphate-buffered saline (DPBS) and Tris-acetate-EDTA (TAE) buffer pH 7 were purchased from ThermoFisher. $MgCl_2$ and NaCl were purchased from Fisher Scientific. Glass coverslips size 1 were purchased from Agar Scientific.

Metal-coated glass substrate preparation for nanopatterning: Glass coverslips were cleaned intensively using our previously published protocol as follows.[35] Coverslips were placed in a Teflon rack, then rinsed with milliQ water (mQ) and carefully sonicated in piranha solution (3:1, sulfuric acid and hydrogen peroxide) inside a small beaker container surrounded by ice for 2 hrs. After this, coverslips were rinsed with mQ and sonicated in mQ for 10 min. Then, coverslips were sonicated in acetone for 10 min, rinsed with mQ, sonicated in ethanol for 10 min, and finally coverslips were blown dry with Argon. After this, cleaned coverslips were loaded into a metal holder for thermal evaporation in vacuum. Metal layers of ~1.5 nm chromium layer (deposition rate of ~0.1 Å/s) as an adhesion layer and ~3.3 nm gold layer (deposition rate of ~0.4 Å/s) on top were deposited as measured by the crystal sensor. After this step, samples were ready for nanopatterning using the FIB equipment.

Top-down Focused Ion Beam (FIB) patterning: Nanoapertures were patterned on the prepared metal-coated glass substrates using the FEI™ Quanta scanning electron microscope and FIB system.[33,54] Apertures' shape were circles with a designed diameter of 200 nm with a spacing distance of 2 μm. Nanopatterned arrays were drawn in the FEI™ Quanta software and milled with a Gallium ion beam of 30 kV/50 pA (or 0.1nA) with a dwelling time tuned to reach the bottom of the nanoaperture. Several arrays of at least 256 nanoapertures were produced in a single substrate. The patterned substrates were characterized immediately using the scanning electron microscope (SEM) capabilities with 5 kV/47 pA, and samples were scanned in AFM afterwards. Patterned substrates were activated with oxygen plasma prior to the biofunctionalization and immobilization of DNA origami.

Bottom-up DNA origami fabrication: The DNA origami used was a triangular-shaped nanostructure called the Rothemund triangle.[30,33,35] This structure was a single-layer DNA sheet with 120 nm side length. It was synthesized by mixing and annealing more than 200 short single-stranded DNAs (called staples) and a 7249-nucleotide circular single-stranded DNA (called scaffold). For simplicity, single-stranded DNA is referred to as ssDNA. During origami preparation some staples were extended to allow hybridization of functional components (see list of sequences in the Supplementary Material). These components were designed to protrude from opposite faces of the DNA origami by selecting DNA duplexes which terminal ends were closer to the face. The staples (100 μM in 1x TAE buffer), the 12 modified staples for biotin anchors, and the biotin-functionalized ssDNAs were mixed in 5:1,

5:1, and 500:1 ratios relative to the scaffold in 1x TAE buffer/12.5 mM Mg^{2+} buffer (called annealing buffer). For ATTO 488 photobleaching experiments, the capturing dye staple and the dye-labeled ssDNA were added in a ratio of 10:1 and 50:1. For protein attachment, the capturing protein staples were added in a ratio of 10:1, while DNA-GFP was added as described in "Protein-DNA origami conjugation" section. The DNA mixture was annealed in a PCR machine (Hybaid Sprint PCR Thermal Cycler, Thermo Scientific) by first heating it to 90 °C for 5 min and cooling it down gradually at the rate of 0.2 °C per min until reaching room temperature. The assembled origami structure was then purified by using microcentrifuge filters (100 kDA MWCO; Millipore Amicon Ultra 0.5) at 10000 rpm three times, 3 minutes each. The final concentration of origami was 1.2 nM in 100 µL annealing buffer. The DNA sequences used for the DNA origami fabrication are included in the Supplementary Material file.

Protein-DNA conjugation and purification: The GFP variant containing 4-azido-l-phenylalanine at residue 204 is based on the superfolding GFP variant and was produced as described previously[53]. GFP protein-DNA conjugation was made via strain-promoted alkyne-azide cycloaddition[55]. The partner to the azide in GFP is bicyclononyne on ssDNA. Briefly, BCN-functionalised DNA (BCN-DNA) was prepared from 3' terminal end amino-functionalised DNA and BCN-NHS ester ((1R,8S,9s)-Bicyclo[6.1.0]non-4-yn-9-ylmethyl N-succinimidyl carbonate, Sigma Aldrich).[55] Azide-functionalized GFP (30 µM) was mixed with BCN-DNA (150 µM) in tris buffer (50 mM; pH 6.8) and let to react overnight in an incubating shaker at 37 °C. The reacted product, i.e. GFP-DNA conjugate, was purified using native (non-denaturing) polyacrylamide gel electrophoresis (PAGE; Biorad Mini-PROTEAN) as follows. A 10% polyacrylamide gel was made, and GFP-DNA was pipetted into the wells. The gel was run in tris-glycine buffer at 150 V. Using a dark light reader (Clare Chemical Research), bands corresponding to GFP-DNA were excised from the gel, frozen, and crushed using a spatula. The crushed bands were soaked in 1x TAE for 48 hrs. The gel was removed from the solution using microcentrifuge filters (Corning; 0.45 µm pore size).

Protein-DNA origami conjugation: After DNA origami and GFP-DNA were assembled and purified in solution, the origami structure (10 nM) was mixed with GFP-DNA (1 µM) in 1x TAE buffer with 12.5 mM $MgCl_2$. The solution was incubated on a shaker at 20 °C for 48 hrs. Excess GFP-DNA was removed by using microcentrifuge filters (100 kDA MWCO; Millipore Amicon Ultra 0.5) at 10000 rpm for 2 min.

Atomic Force Microscopy (AFM): DNA origami-GFP conjugates were characterized using AFM in fluid. A Bruker Dimension Icon AFM was used in PeakForce QNM mode with ScanAsyst Fluid probes. Origami – either before or after centrifugal filtering – was deposited on freshly cleaved mica. Imaging conditions were critical to unambiguously distinguish proteins attached to the origamis. The imaging was carried out in water with 50 mM Mg^{2+}. In a typical experiment, the origamis were localized at a scan rate of 2 Hz with 256 samples/line. When a region of interest was found, the scan rate was reduced to 0.5 Hz and samples/line was increased to 512. The setpoint was minimized to avoid the denaturation of the DNA origami-GFP conjugate. Images were processed in Bruker Nanoscope Analysis software. DNA origami-GFP and patterns were also characterized with AFM in air using the

same AFM equipment but with ScanAsyst Air tips (tip radius 12 nm) in tapping mode with 512 samples per line and a scan rate of 0.5 Hz. In case of origamis, the sample solution was deposited onto a piece of freshly cleaved mica and rinsed with water, and then immersed in ethanol and dried before AFM measurement.

Immobilization of Cy5-labeled DNA duplexes in the nanoarrays: Substrate was plasma cleaned for 15 min, and subsequently they were allowed to cool to room temperature. The carbodiimide coupling was performed as follows. 1% CTES (carboxyethylsilanetriol di-sodium salt; Gelest) in 10mM Tris pH 8.3 was casted on the substrate for 1 h in a shaker. Then, the substrate was rinsed with mQ and blow dry with Argon. Substrate was baked at 90 °C for 1.5 hrs. Then, a solution of 100 mM EDC (1-Ethyl-3-(3-dimethylaminopropyl) carbodiimide; from Sigma-Aldrich) and 200 mM Sulfo-NHS (from Thermofisher) in mQ was casted on the substrate for 1 h in a shaker and rinsed with mQ leaving a volume of about 100 µl on top of the pattern. A solution containing an amine-functionalized ssDNA (1 µM) and its complementary Cy5-labeled ssDNA (1 µM) in 40 µM $MgCl_2$ was cast on top of the pattern for 1 h at room temperature. Substrates were rinsed with 1x DBPS and stored overnight. Before Total Internal Reflection Fluorescence (TIRF) microscopy, substrates were blow dried with argon.

Immobilization of the DNA origami in the nanoarrays: Substrate was plasma cleaned for 20 min, and subsequently they were allowed to cool to room temperature. Cloning cylinders were glued (ethyl 2-cyano acrylate; Loctite) to the cleaned substrates in order to be used as reaction chambers or wells. 0.1 mg/µL PEG (Biotin-PEG-Silane, MW 3,400, 500 mg; Laysan Bio) in 95% ethanol was added and incubated for 1.5 hrs. We then rinsed with mQ water. 0.1 mg/mL streptavidin (ThermoFisher) was added and incubated for 0.5 h; we rinsed with mQ water, and exchanged to 1× TAE buffer/12.5 mM Mg^{2+}. 2.4 nM functionalized, biotinylated origami was added and incubated for 0.5 hrs. Subsequently the samples were rinsed with 1x DPBS, which we believe help preventing non-specific adsorption of DNA origamis to the gold nanoarray[18]. Buffer was exchanged back to 1× TAE/12.5 mM Mg^{2+}.

Total Internal Reflection Fluorescence (TIRF) Microscopy: Single-molecule monitoring was performed using an LSM710 ELYRA PS.1 in TIRF mode with a 642 nm (150 mW) or 488 nm (100 mW) laser excitation. Cy5 nanoarrays were observed with 642 nm at 0.05% laser power and 100 ms camera acquisition time. Single dye nanoarrays were monitored with 5% laser power and 500 ms acquisition time in a 1x DBPS buffer containing 450 mM NaCl (final concentration), 4.15 mM $MgCl_2$, 2% Tween 20 (from Sigma-Aldrich), Trolox (from Sigma-Aldrich), and oxygen scavenger (1 mg/mL glucose oxidase and 0.4% v/v catalase, from Sigma-Aldrich). For photobleaching experiments, laser power was increased to 100%. Single protein nanoarrays were monitored with 488 nm at 2-5% laser power, BP495-550 filter and 50-100 ms camera acquisition time.

Analysis of TIRF Microscopy: Using ImageJ, we analyzed a TIRF microscopy time lapse (see the Supplementary Material for representative frames). Initially, a time lapse was loaded into ImageJ as a Stack. Then, bright spots were visually identified. A 2x2 pixels region was selected on the bright spot and shifted around the spot in such a way that the maximum intensity was obtained using the ImageJ's Plot Z-axis Profile tool. We judged the

presence of fluorescence by comparing the intensity in the expected position of the nanoaperture with the background intensity upon bleaching or the background intensity of the surroundings using the image analysis software ImageJ.

III. RESULTS

In this work, nanoarrays were initially patterned on a Gold/Chromium metal-coated glass substrate (Figure 1a) with a single Focused Ion Beam (FIB) step, as described previously.[6,33] In this FIB step, a pattern consisting of nanoapertures with a diameter *ø* and with lattice periodicity *d* were milled (Figure 1b). This strategy allowed exposure of the glass surface beneath the metal-coating for further passivation and biofunctionalization using DNA origami tile structures. To control the process with single-molecule resolution, DNA origami nanostructures were designed to each display a single fluorescent molecule on one face via a ssDNA anchor (the addressable element), and were then cast and immobilised onto the nanoapertures via molecular anchors on the opposite face using biotin with streptavidin as a linker between the origami structure and the biotin-silanized glass surface (Figure 1c).

A representative AFM image of the nanoaperture array (*ø* = 200 nm, with d = 2 μm) is shown in Figure 2a with the height profile indicating successful formation of the nanoapertures. Additional pattern characterization using scanning electron microscope (SEM) is shown in Figure SM1 in the Supplementary Material. We confirmed whether the nanoapertures were available for functionalisation by attaching fluorescent dye molecules. Cy5-modified DNA duplexes were immobilized on the nanoapertures' exposed glass via EDC/Sulfo-NHS carbodiimide coupling (see Methods). TIRF microscopy confirmed the formation of a Cy5 nanoarray with ~100% yield (Figure 2b).

To probe that our nanoarray fabrication strategy was suitable for single molecule monitoring, we immobilized triangular DNA origami nanostructures designed to present a single dye (see Methods). An ATTO 488 dye was selected as its excitation and emission spectra are similar to green fluorescent proteins (GFPs). The actual DNA origami structure is shown in Figure 3a. The dimension of the triangular nanostructure is 120 nm per side, by design, so only 1 structure can in principle physically fit per well. Furthermore, the face of the structure presented was defined through biotin anchors (Figure 1c). In contrast to previous origami immobilization methods,[32,33,56] we chose to use biotin anchors on one origami's face to ensure the dye, and ultimately the protein, would be protruding from the other face and exposed to the buffer solution. The biotin anchors were achieved by hybridizing a unique biotin-functionalized ss DNA with 12 ssDNA anchors on the origami's face. A single ATTO 488-functionalised oligonucleotide was immobilized via DNA hybridization to the single available complementary ssDNA on the triangular DNA origami tile (schematic in Figure 3b).[57,58] Next, the biotinylated DNA origami construct was immobilized onto the nanoarrays by casting them onto nanoapertures, which were previously functionalised with PEG-biotin and streptavidin for passivation (see Methods).

Total internal reflection fluorescence (TIRF) microscopy showed that 88% of the nanoapertures had observable fluorescence, hereinafter called bright spots, indicative of nanoapertures occupied by DNA origami nanostructures (Figure 3c). We observed that bright spots occur in the background too, but the majority were present in the nanoaperture. Photobleaching experiments indicated that 85.9% of bright spots had a single photobleaching step (high to low intensity transition as seen in the representative trace in Figure 3c. See also additional traces in Figure SM2). The histogram of the step bleaching (Figure SM3) shows that the majority of dyes can be monitored for a time window of at least 20 sec. One-step bleaching events strongly suggested that single dye molecules were present in each nanoaperture, thus single DNA nanostructures were immobilized in each nanoaperture; 3.1% of the bright spots exhibited two-step photobleaching, suggesting the presence of two dyes, and hence, double DNA nanostructure occupancy. 10.9% of the bright spots had diverse single-step transition events which still suggests single occupancy (see ref. note[59] and representative traces in Figure SM4). All in all, 97% of nanoapertures with bright spots had single DNA origami structures immobilized. While, in the context of the entire nanoarray, 85% of the nanoapertures had single occupancy of DNA origami structures.

To fabricate single protein nanoarrays, we attached individual green fluorescent protein (GFP) molecules onto DNA origami nanostructure. We have previously engineered GFP to contain azide chemistry close to the chromophore (residue 204; see Figure 4a) using a reprogramed genetic approach[28,52,53,55]. Incorporation of azide chemistry via the non-canonical amino acid 4-azido-l-phenyalalanine (AzF) provides a means to link the addressing ssDNA to the protein in a single designed site via strain promoted alkyne-azide cycloaddition (SPAAC). This in turn generates a homogenous protein-DNA origami structure system which is essential for monitoring single molecule events; due to the high prevalence of lysine residues on a protein's surface, primary amine attachment processes (i.e. lysine residues) would generate a highly heterogenous system with each well on the array representing different protein-DNA origami structure configurations and potentially functional effects. GFP with azide at residue 204 (here on called GFP^{204AzF}) was linked to ssDNA using SPAAC; the addressing ssDNA was modified with BCN at its 3' end allowing SPAAC to occur simply on mixing the two molecules (Figure 4a). The DNA-GFP product was then purified (see Methods). Subsequently, the DNA-GFP conjugate was incubated in solution with the DNA origami, which had a protruding complementary ssDNA that allowed tethering of the DNA-GFP to the DNA origami structure. Previous work has shown that attachment of BCN ssDNA to GFP^{204AzF} has little effect on the bulk spectral properties of GFP[28].

After incubation, GFP^{AzF204}-functionalised origami nanostructures (GFP-origami hereinafter) were purified. We tested two positions on the nanostructure for the GFP tethering: on the origami edge and on the (top) face (schemes in Figures 4b and 4c, respectively). AFM images of the GFP-origami structures obtained in liquid and air confirmed the successful functionalization of GFP on DNA origami in a 1:1 ratio; representative AFM images are shown in Figures 4b and 4c (see Figure SM5 and SM6 for additional AFM images). We found 54.7% of DNA origami had GFP conjugated to the structures from a sample size of 53 across several preparations. Imaging conditions were critical to

unambiguously distinguish proteins in liquid attached to the origamis requiring higher ionic concentrations in the imaging buffer (see also Figure SM7) and selection of appropriate AFM tips (see Methods). Moreover, the fluid-mode AFM process is dynamic, where proteins may be displaced in the course of imaging.

We then immobilized the GFP-origami structures into the nanoarrays via the aforementioned biotin-streptavidin method. TIRF microscopy showed that 54% of nanoapertures exhibited fluorescent spots (Figure 5a), in agreement with the yield observed via AFM. A representative single nanoaperture's intensity over time depicting the GFP photo-blinking behavior is shown in Figure 5(b) – this on/off blinking behavior has been attributed to the charged state of GFP's chromophore, but the exact cause of the intermittent blinking is unknown[60,61]. The intensity traces were in line with a previous single molecule analysis of GFP^{AzF204} (see Figure SM8 for additional intensity traces).[62] Overall these results demonstrate that single proteins can be spatially arranged over large areas using our combined fabrication strategy. The lower yield of protein occupancy in the nanoapertures obtained with our DNA origami nanoarrays compared to the aforementioned DNA origami-dye arrays (Figure 3) is likely ascribable to increased steric hindrance and electrostatic interactions between the protein and DNA origami

IV. CONCLUSIONS

Monitoring single protein molecule events requires overcoming various challenges. The first is represented by the constrain of a single protein molecule to a defined area. We achieved this here combining the functionalisation of DNA origami with individual proteins and their fixed organization in FIB nanopatterned wells for long-term monitoring. As the wells will potentially hold several proteins molecules of the size of GFP, to achieve single protein molecules per well, we successfully employed DNA origami nanostructures with direction functionality: one face to bind to the well surface and the other to present a sequence for attaching a single incoming protein. The final challenge is the nature of the protein-DNA nanostructure interface. For single molecule experiments, the conjugation between the protein and the underlying supporting material (in this case DNA origami structure) should ideally be defined, designed and homogenous so only a single population of protein species is being observed. Without such control multiple different orientations and configurations will be observed with the positions of attachments making data interpretation difficult and potentially affecting function (e.g. changing active site access, structure and dynamics). We have addressed this challenge here by using a reprogrammed genetic code to engineer into a protein new chemistry not present in nature to allow residue-specific linkage to an addressable ssDNA unit via bioorthogonal click chemistry (SPAAC in this case). The result is a nanoarray system where the contents of each well are highly defined and uniform in terms of their molecular arrangement. Direct quantification of the occupancy of the single molecule into the nanoapertures was provided, demonstrating an excellent yield comparable to other nanoarray methods[27,63].

The single-molecule fabrication strategy we presented is of general applicability for the fabrication of high-throughput and automated addressable protein biochips that can allow the investigation, with single-molecule control, of biomolecular events such as aptamer-biomarker recognition,[35,64] protein-DNA interactions (e.g. CRISPR),[65] protein-protein interactions,[66] enzyme (cascade) reactions,[67–69] and general biosensing and biomimetic assays.[48,70,71] For instance, relevant components could be introduced into the DNA nano-breadboard for the development of biosensor nanoarrays supported by current advances in protein engineering.[72] Moreover, the nanoarrays configuration can allow for the development of high-throughput DNA platforms for super-resolution standards.[73,74] Finally, the strategy we presented can be applied to a myriad of (bio)physical studies that take advantage of the programmability of DNA origami[38]; these include: tracking cellular forces,[75] the use of stimuli-responsive DNA-powered structures[76,77] for the construction of in-vitro DNA nanodevices,[78] as well as for the development of quantum-related applications,[79,80] DNA computing circuits[81,82], and information coding.[83,84]

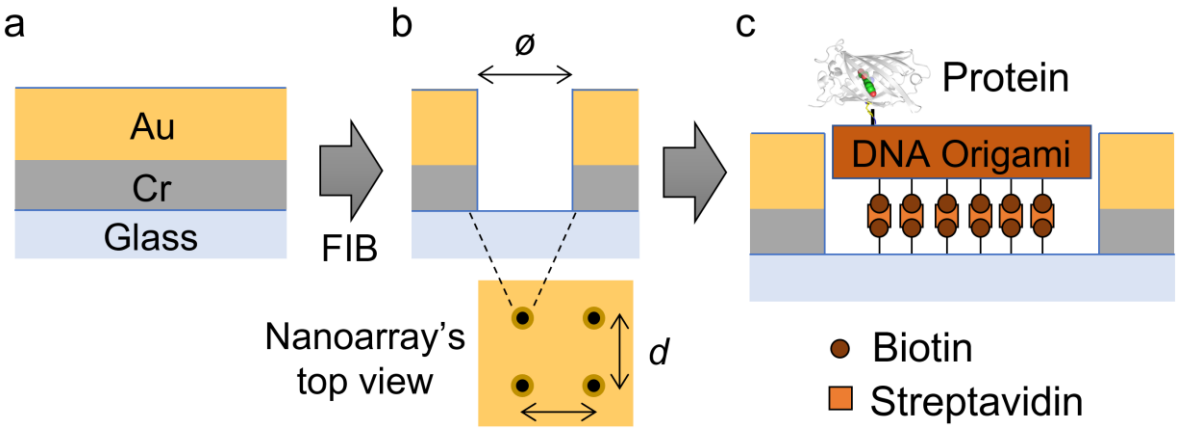

Figure 1. Schematic of the fabrication of nanoarrays for single molecule experiments. (a) A metal-coated glass is prepared on a glass substrate via evaporation of gold and chromium as intermediate adhesive layer. (b) Patterning via a single-step FIB. Nanoapertures of a selected diameter *ø* and spaced an optically-resolvable distance *d* were drilled through the metallic layers until reaching the glass substrate surface. (c) Biofunctionalization and passivation of the exposed glass surface and placement of the protein-conjugated DNA origami nanostructure, which was biotinylated on one face for attachment to the bottom of the nanoaperture.

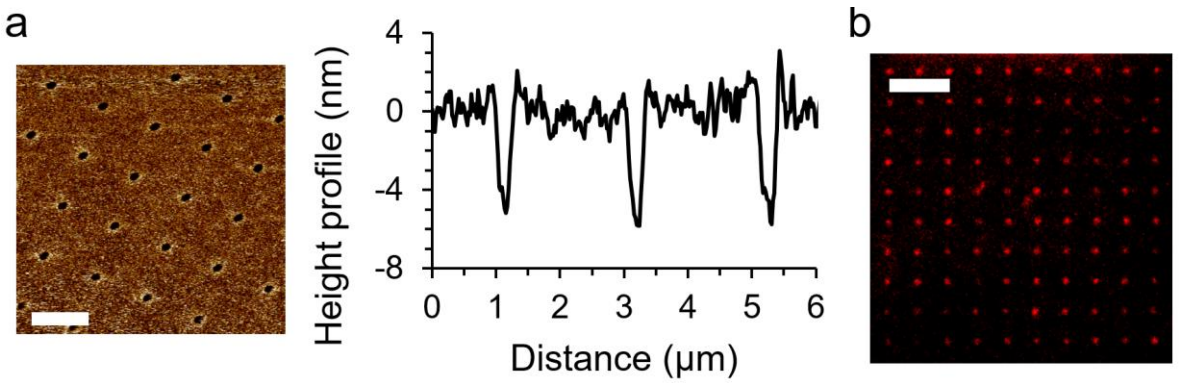

Figure 2. Characterization of nanoarrays patterned via FIB. (a) AFM topography image and height profile of the nanoapertures. (b) TIRF microscopy of Cy5-labeled DNA duplexes covalently tethered to the nanoapertures. This image is a single frame captured at 100 ms with the 642 nm laser. Scale bars in (a) and (b) are 2 μm and 4 μm, respectively.

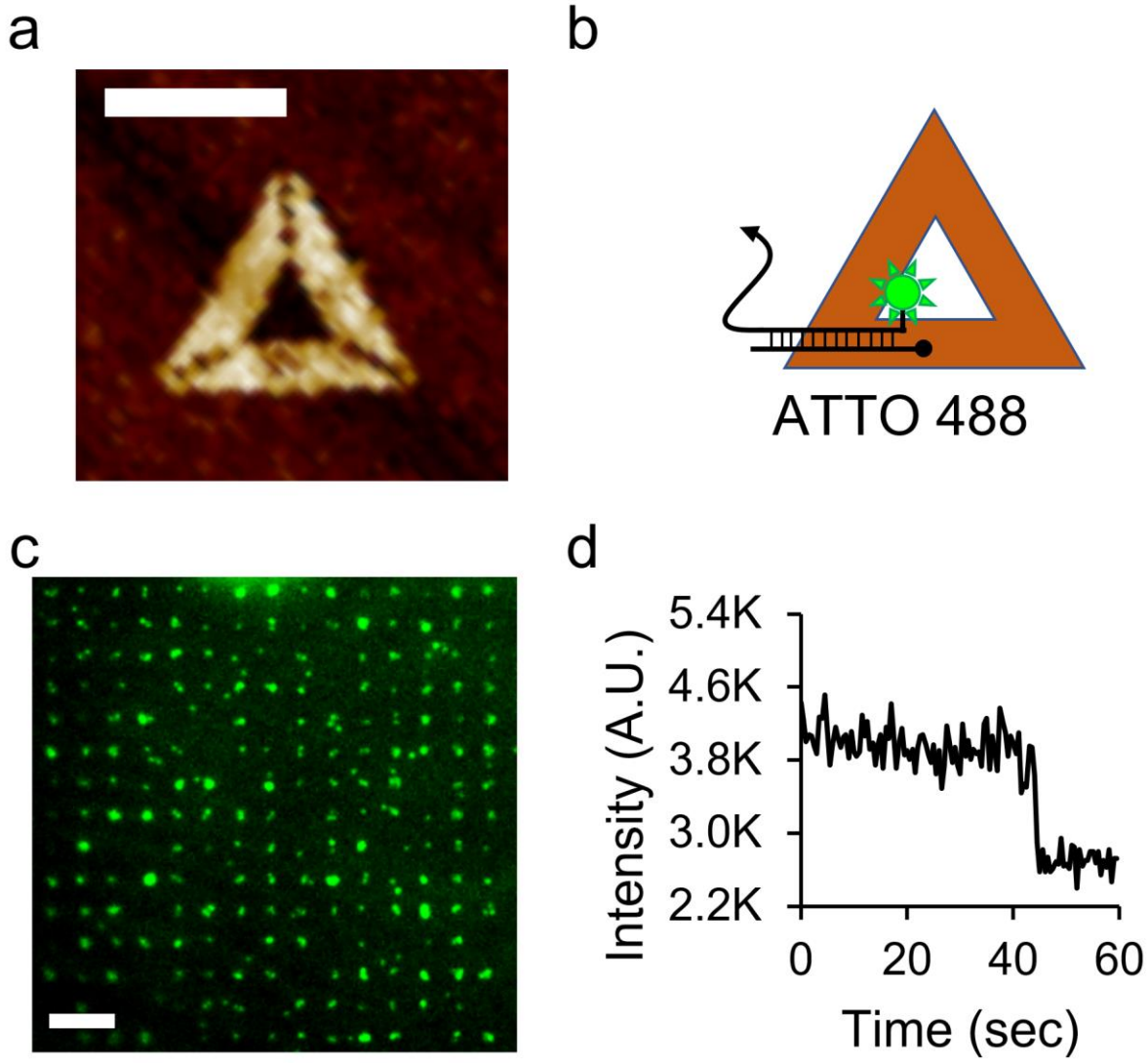

Figure 3. Single dye nanoarrays. (a) DNA origami. (b) Functionalisation of DNA origami with a single ATTO 488 dye on its face. (c) TIRF microscopy of nanoarray of single dyes. Captured with 488 nm laser and camera acquisition time of 500 ms. This image is the summation over 10 frames. (d) Representative single photobleaching step of a spot in the nanoarray. The dimension of the DNA anchor in (b) is oversized. Scale bars in (a) and (c) are 100 nm and 4 μm, respectively.

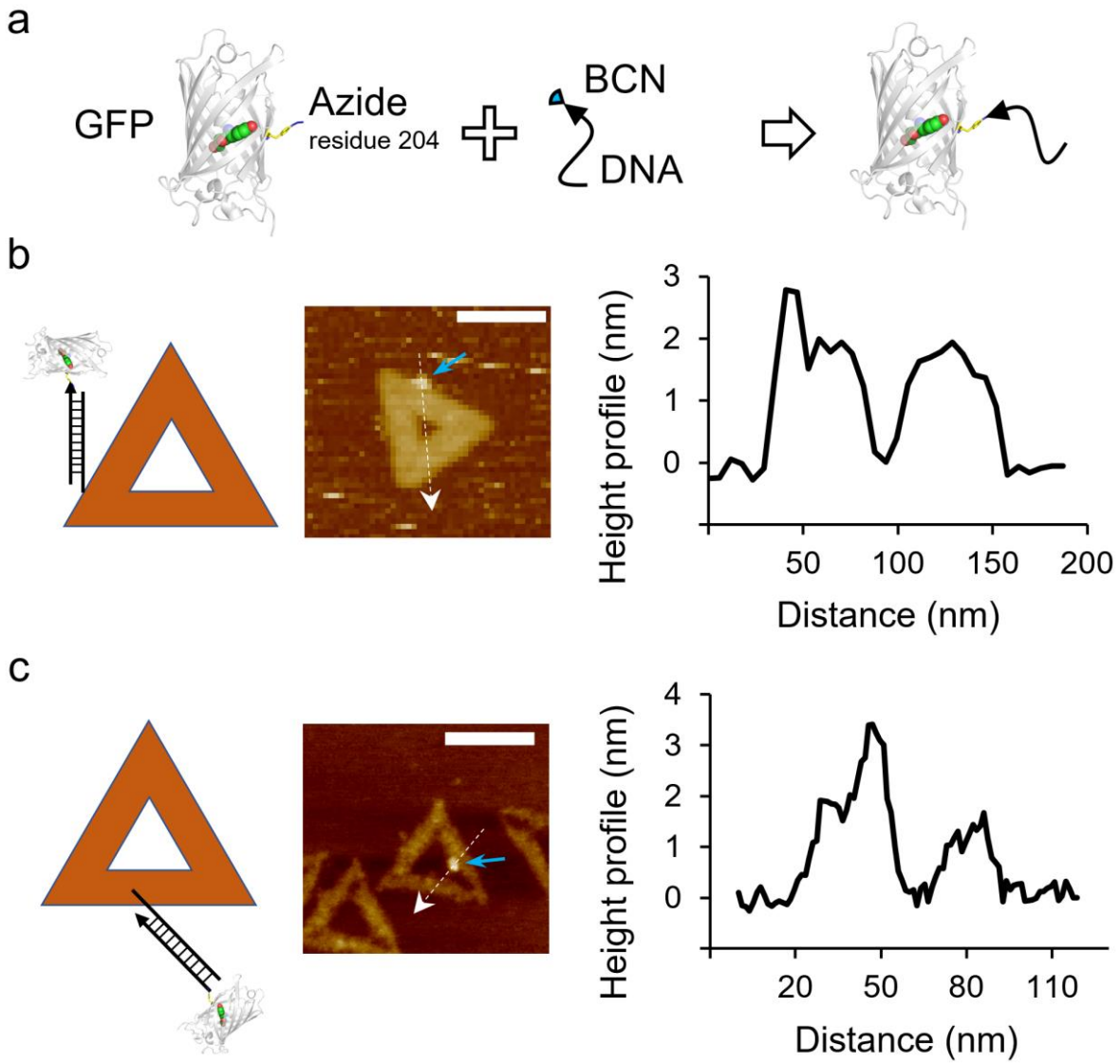

Figure 4. (a) Fabrication of DNA-modified GFP protein via click chemistry based on azide and BCN functional groups. The azide at residue 204 in the short axis of the protein and the chromophore (green and red atoms inside the GFP) are shown. (b) Schematic of the single protein placement in the edge of the DNA origami, a representative image of AFM in liquid, and height profile along the white arrow, and blue arrow indicates the position of the protein. Additional structures from AFM are shown in Figure SM4. (c) Schematic of the single protein placement on the face of the DNA origami, a representative image of AFM in air, height profile along the white arrow, and blue arrow indicate the position of the protein; the profile indicates the size of the protein is ~1.5 nm in air. The dimensions of the DNA anchors in (b) and (c) are oversized. Scale bars are 100 nm.

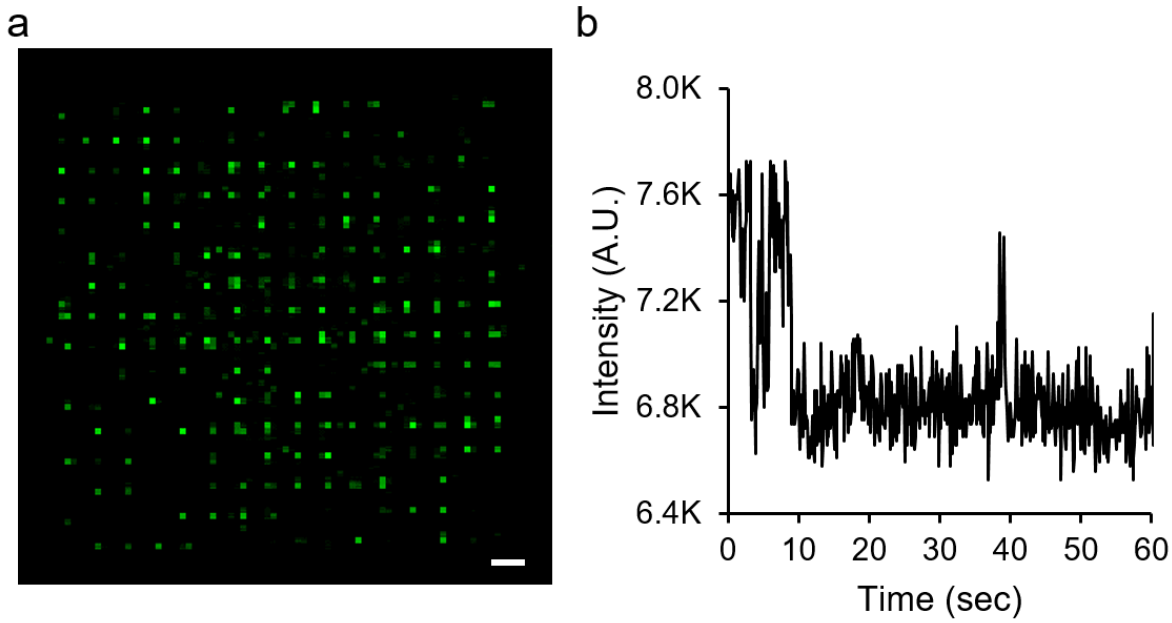

Figure 5. (a) TIRF microscopy of nanoarray of single GFP proteins attached to DNA origami on its face. Captured with 488 nm laser and camera acquisition time of 100 ms. This image was taken with 4x4 binning and shows the maximum intensities over the time lapse. (b) Representative photo-blinking event of a GFP in a nanoarray, which is characteristic of the GFP protein. Scale bar is 2 μm.

SUPPLEMENTARY MATERIAL

See the supplementary material for the additional detailed AFM, TIRF images and the DNA sequences.

ACKNOWLEDGMENTS

The authors gratefully acknowledge financial support from the Air Force Office of Scientific Research under award FA9550-17-1-0179. REAG is supported by the BBSRC-funded South West Biosciences Doctoral Training Partnership [training grant reference BB/M009122/1]. For the purpose of open access, the author has applied a creative commons attribution (CC BY) licence (where permitted by UKRI, ‘open government licence’ or ‘creative commons attribution no-derivatives (CC BY-ND) licence’ may be stated instead) to any author accepted manuscript version arising."

REFERENCES

(1) Drmanac, R.; Sparks, A. B.; Callow, M. J.; Halpern, A. L.; Burns, N. L.; Kermani, B. G.; Carnevali, P.; Nazarenko, I.; Nilsen, G. B.; Yeung, G.; Dahl, F.; Fernandez, A.; Staker, B.; Pant, K. P.; Baccash, J.; Borcherding, A. P.; Brownley, A.; Cedeno, R.; Chen, L.; Chernikoff, D.; Cheung, A.; Chirita, R.; Curson, B.; Ebert, J. C.; Hacker, C. R.; Hartlage, R.; Huser, B.; Huang, S.; Jiang, Y.; Karpinchyk, V.; Koenig, M.; Kong, C.; Landers, T.; Le, C.; Liu, J.; McBride, C. E.; Morenzoni, M.; Morey, R. E.; Mutch, K.; Perazich, H.; Perry, K.; Peters, B. A.; Peterson, J.; Pethiyagoda, C. L.; Pothuraju, K.; Richter, C.; Rosenbaum, A. M.; Roy, S.; Shafto, J.; Sharanhovich, U.; Shannon, K. W.; Sheppy, C. G.; Sun, M.; Thakuria, J. v.; Tran, A.; Vu, D.; Zaranek, A. W.; Wu, X.; Drmanac, S.; Oliphant, A. R.; Banyai, W. C.; Martin, B.; Ballinger, D. G.; Church, G. M.; Reid, C. A. Human Genome Sequencing Using Unchained Base Reads on Self-Assembling DNA Nanoarrays. *Science* **2010**, *327* (5961), 78–81. https://doi.org/10.1126/SCIENCE.1181498.

(2) Ishijima, A.; Yanagida, T. Single Molecule Nanobioscience. *Trends in Biochemical Sciences* **2001**, *26* (7), 438–444. https://doi.org/10.1016/S0968-0004(01)01860-6.

(3) Palma, M.; Abramson, J. J.; Gorodetsky, A. A.; Penzo, E.; Gonzalez, R. L.; Sheetz, M. P.; Nuckolls, C.; Hone, J.; Wind, S. J. Selective Biomolecular Nanoarrays for Parallel Single-Molecule Investigations. *J Am Chem Soc* **2011**, *133* (20), 7656–7659. https://doi.org/10.1021/JA201031G.

(4) Smiley, R. D.; Hammes, G. G. Single Molecule Studies of Enzyme Mechanisms. *Chemical Reviews* **2006**, *106* (8), 3080–3094. https://doi.org/10.1021/CR0502955.

(5) Angelin, A.; Weigel, S.; Garrecht, R.; Meyer, R.; Bauer, J.; Kumar, R. K.; Hirtz, M.; Niemeyer, C. M. Multiscale Origami Structures as Interface for Cells. *Angewandte Chemie International Edition* **2015**, *54* (52), 15813–15817. https://doi.org/10.1002/anie.201509772.

(6) Huang, D.; Patel, K.; Perez-Garrido, S.; Marshall, J. F.; Palma, M. DNA Origami Nanoarrays for Multivalent Investigations of Cancer Cell Spreading with Nanoscale Spatial Resolution and Single-Molecule Control. *ACS Nano* **2019**, *13* (1), 728–736. https://doi.org/10.1021/acsnano.8b08010.

(7) Li, Y.; Zhang, J.; Liu, W.; Li, D.; Fang, L.; Sun, H.; Yang, B. Hierarchical Polymer Brush Nanoarrays: A Versatile Way to Prepare Multiscale Patterns of Proteins. *ACS Applied Materials and Interfaces* **2013**, *5* (6), 2126–2132. https://doi.org/10.1021/AM3031757.

(8) Kielar, C.; Reddavide, F. V.; Tubbenhauer, S.; Cui, M.; Xu, X.; Grundmeier, G.; Zhang, Y.; Keller, A. Pharmacophore Nanoarrays on DNA Origami Substrates as a Single-Molecule Assay for Fragment-Based Drug Discovery. *Angewandte Chemie* **2018**, *130* (45), 15089–15093. https://doi.org/10.1002/ange.201806778.

(9) Blum, C.; Cesa, Y.; Escalante, M.; Subramaniam, V. Multimode Microscopy: Spectral and Lifetime Imaging. *Journal of The Royal Society Interface* **2008**, *6* (Suppl_1), S35–S43. https://doi.org/10.1098/RSIF.2008.0356.FOCUS.

(10) Ahn, J. H.; Kim, J. H.; Reuel, N. F.; Barone, P. W.; Boghossian, A. A.; Zhang, J.; Yoon, H.; Chang, A. C.; Hilmer, A. J.; Strano, M. S. Label-Free, Single Protein Detection on a near-Infrared Fluorescent Single-Walled Carbon Nanotube/Protein Microarray Fabricated by Cell-Free Synthesis. *Nano Letters* **2011**, *11* (7), 2743–2752. https://doi.org/10.1021/NL201033D.

(11) Dong, J.; Salem, D. P.; Sun, J. H.; Strano, M. S. Analysis of Multiplexed Nanosensor Arrays Based on Near-Infrared Fluorescent Single-Walled Carbon Nanotubes. *ACS Nano* **2018**, *12* (4), 3769–3779. https://doi.org/10.1021/ACSNANO.8B00980.

(12) Yu, X.; Xu, D.; Cheng, Q. Label-Free Detection Methods for Protein Microarrays. *PROTEOMICS* **2006**, *6* (20), 5493–5503. https://doi.org/10.1002/PMIC.200600216.

(13) Christman, K. L.; Schopf, E.; Broyer, R. M.; Li, R. C.; Chen, Y.; Maynard, H. D. Positioning Multiple Proteins at the Nanoscale with Electron Beam Cross-Linked Functional Polymers. *J Am Chem Soc* **2009**, *131* (2), 521–527. https://doi.org/10.1021/ja804767j.

(14) Li, S.; Zeng, S.; Chen, L.; Zhang, Z.; Hjort, K.; Zhang, S.-L. Nanoarrays on Passivated Aluminum Surface for Site-Specific Immobilization of Biomolecules. *ACS Applied Bio Materials* **2018**, *1* (1), 125–135. https://doi.org/10.1021/acsabm.8b00037.

(15) Yang, W.; van Dijk, M.; Primavera, C.; Dekker, C. FIB-Milled Plasmonic Nanoapertures Allow for Long Trapping Times of Individual Proteins. *iScience* **2021**, *24* (11), 103237. https://doi.org/10.1016/J.ISCI.2021.103237.

(16) Schvartzman, M.; Palma, M.; Sable, J.; Abramson, J.; Hu, X.; Sheetz, M. P.; Wind, S. J. Nanolithographic Control of the Spatial Organization of Cellular Adhesion Receptors at the Single-Molecule Level. *Nano Letters* **2011**, *11* (3), 1306–1312. https://doi.org/10.1021/nl104378f.

(17) Lum, W.; Gautam, D.; Chen, J.; Sagle, L. B. Single Molecule Protein Patterning Using Hole Mask Colloidal Lithography. *Nanoscale* **2019**, *11* (35), 16228–16234. https://doi.org/10.1039/C9NR05630K.

(18) Brassat, K.; Ramakrishnan, S.; Bürger, J.; Hanke, M.; Doostdar, M.; Lindner, J. K. N.; Grundmeier, G.; Keller, A. On the Adsorption of DNA Origami Nanostructures in Nanohole Arrays. *Langmuir* **2018**, *34* (49), 14757–14765. https://doi.org/10.1021/ACS.LANGMUIR.8B00793.

(19) Liu, X.; Kumar, M.; Calo, A.; Albisetti, E.; Zheng, X.; Manning, K. B.; Elacqua, E.; Weck, M.; Ulijn, R. v.; Riedo, E. High-Throughput Protein Nanopatterning. *Faraday Discussions* **2019**, *219* (0), 33–43. https://doi.org/10.1039/C9FD00025A.

(20) Lee, S. W.; Oh, B.-K.; Sanedrin, R. G.; Salaita, K.; Fujigaya, T.; Mirkin, C. A. Biologically Active Protein Nanoarrays Generated Using Parallel Dip-Pen Nanolithography. *Advanced Materials* **2006**, *18* (9), 1133–1136. https://doi.org/10.1002/adma.200600070.

(21) Biswas, K. H.; Cho, N.-J.; Groves, J. T. Fabrication of Multicomponent, Spatially Segregated DNA and Protein-Functionalized Supported Membrane Microarray. *Langmuir* **2018**, *34* (33), 9781–9788. https://doi.org/10.1021/acs.langmuir.8b01364.

(22) Lindner, M.; Tresztenyak, A.; Fülöp, G.; Jahr, W.; Prinz, A.; Prinz, I.; Danzl, J. G.; Schütz, G. J.; Sevcsik, E. A Fast and Simple Contact Printing Approach to Generate 2D Protein Nanopatterns. *Frontiers in Chemistry* **2019**, *6*, 655. https://doi.org/10.3389/fchem.2018.00655.

(23) Schneider, A. K.; Nikolov, P. M.; Giselbrecht, S.; Niemeyer, C. M. DNA-SMART: Biopatterned Polymer Film Microchannels for Selective Immobilization of Proteins and Cells. *Small* **2017**, *13* (17), 1603923. https://doi.org/10.1002/SMLL.201603923.

(24) Carbonell, C.; Valles, D.; Wong, A. M.; Carlini, A. S.; Touve, M. A.; Korpanty, J.; Gianneschi, N. C.; Braunschweig, A. B. Polymer Brush Hypersurface Photolithography. *Nature Communications 2020 11:1* **2020**, *11* (1), 1–8. https://doi.org/10.1038/s41467-020-14990-x.

(25) Singh, G.; Gohri, V.; Pillai, S.; Arpanaei, A.; Foss, M.; Kingshott, P. Large-Area Protein Patterns Generated by Ordered Binary Colloidal Assemblies as Templates. *ACS Nano* **2011**, *5* (5), 3542–3551. https://doi.org/10.1021/NN102867Z.

(26) Cai, Y.; Ocko, B. M. Large-Scale Fabrication of Protein Nanoarrays Based on Nanosphere Lithography. *Langmuir* **2005**, *21* (20), 9274–9279. https://doi.org/10.1021/LA051656E.

(27) Shetty, R. M.; Brady, S. R.; Rothemund, P. W. K.; Hariadi, R. F.; Gopinath, A. Bench-Top Fabrication of Single-Molecule Nanoarrays by DNA Origami Placement. *ACS Nano* **2021**, *15* (7), 11441–11450. https://doi.org/10.1021/ACSNANO.1C01150.

(28) Marth, G.; Hartley, A. M.; Reddington, S. C.; Sargisson, L. L.; Parcollet, M.; Dunn, K. E.; Jones, D. D.; Stulz, E. Precision Templated Bottom-Up Multiprotein Nanoassembly through Defined Click Chemistry Linkage to DNA. *ACS Nano* **2017**, *11* (5), 5003–5010. https://doi.org/10.1021/acsnano.7b01711.

(29) Dong, Y.; Mao, Y. DNA Origami as Scaffolds for Self-assembly of Lipids and Proteins. *ChemBioChem* **2019**, 2422–2431. https://doi.org/10.1002/cbic.201900073.

(30) Rothemund, P. W. K. Folding DNA to Create Nanoscale Shapes and Patterns. *Nature 2006 440:7082* **2006**, *440* (7082), 297–302. https://doi.org/10.1038/nature04586.

(31) Rosier, B. J. H. M.; Cremers, G. A. O.; Engelen, W.; Merkx, M.; Brunsveld, L.; De Greef, T. F. A. Incorporation of Native Antibodies and Fc-Fusion Proteins on DNA Nanostructures via a

Modular Conjugation Strategy. *Chemical Communications* **2017**, *53* (53), 7393–7396. https://doi.org/10.1039/C7CC04178K.

(32) Gopinath, A.; Rothemund, P. W. K. Optimized Assembly and Covalent Coupling of Single-Molecule DNA Origami Nanoarrays. *ACS Nano* **2014**, *8* (12), 12030–12040. https://doi.org/10.1021/nn506014s.

(33) Huang, D.; Freeley, M.; Palma, M. DNA-Mediated Patterning of Single Quantum Dot Nanoarrays: A Reusable Platform for Single-Molecule Control. *Scientific Reports* **2017**, *7* (1), 45591. https://doi.org/10.1038/srep45591.

(34) Hawkes, W.; Huang, D.; Reynolds, P.; Hammond, L.; Ward, M.; Gadegaard, N.; Marshall, J. F.; Iskratsch, T.; Palma, M. Probing the Nanoscale Organisation and Multivalency of Cell Surface Receptors: DNA Origami Nanoarrays for Cellular Studies with Single-Molecule Control. *Faraday Discussions* **2019**, *219* (0), 203–219. https://doi.org/10.1039/C9FD00023B.

(35) Cervantes-Salguero, K.; Freeley, M.; Chávez, J. L.; Palma, M. Single-Molecule DNA Origami Aptasensors for Real-Time Biomarker Detection. *Journal of Materials Chemistry B* **2020**, *8* (30), 6352–6356. https://doi.org/10.1039/D0TB01291B.

(36) Ngo, T. A.; Dinh, H.; Nguyen, T. M.; Liew, F. F.; Nakata, E.; Morii, T. Protein Adaptors Assemble Functional Proteins on DNA Scaffolds. *Chemical Communications* **2019**, *55* (83), 12428–12446. https://doi.org/10.1039/C9CC04661E.

(37) Hager, R.; Burns, J. R.; Grydlik, M. J.; Halilovic, A.; Haselgrübler, T.; Schäffler, F.; Howorka, S. Co-Immobilization of Proteins and DNA Origami Nanoplates to Produce High-Contrast Biomolecular Nanoarrays. *Small* **2016**, *12* (21), 2877–2884. https://doi.org/10.1002/SMLL.201600311.

(38) Cervantes-Salguero, K.; Biaggne, A.; Youngsman, J. M.; Ward, B. M.; Kim, Y. C.; Li, L.; Hall, J. A.; Knowlton, W. B.; Graugnard, E.; Kuang, W. Strategies for Controlling the Spatial Orientation of Single Molecules Tethered on DNA Origami Templates Physisorbed on Glass Substrates: Intercalation and Stretching. *International Journal of Molecular Sciences* **2022**, *23* (14), 7690. https://doi.org/10.3390/IJMS23147690.

(39) Wong, L. S.; Khan, F.; Micklefield, J. Selective Covalent Protein Immobilization: Strategies and Applications. *Chemical Reviews* **2009**, *109* (9), 4025–4053. https://doi.org/10.1021/cr8004668.

(40) Jonkheijm, P.; Weinrich, D.; Schröder, H.; Niemeyer, C. M.; Waldmann, H. Chemical Strategies for Generating Protein Biochips. *Angewandte Chemie International Edition* **2008**, *47* (50), 9618–9647. https://doi.org/10.1002/anie.200801711.

(41) Seeman, N. C. Nanomaterials Based on DNA. *Annual Review of Biochemistry* **2010**, *79*, 65–87. https://doi.org/10.1146/ANNUREV-BIOCHEM-060308-102244.

(42) Schnitzbauer, J.; Strauss, M. T.; Schlichthaerle, T.; Schueder, F.; Jungmann, R. Super-Resolution Microscopy with DNA-PAINT. *Nature Protocols 2017 12:6* **2017**, *12* (6), 1198–1228. https://doi.org/10.1038/nprot.2017.024.

(43) Huang, J.; Suma, A.; Cui, M.; Grundmeier, G.; Carnevale, V.; Zhang, Y.; Kielar, C.; Keller, A. Arranging Small Molecules with Subnanometer Precision on DNA Origami Substrates for the Single-Molecule Investigation of Protein–Ligand Interactions. *Small Structures* **2020**, *1* (1), 2000038. https://doi.org/10.1002/SSTR.202000038.

(44) Funke, J. J.; Dietz, H. Placing Molecules with Bohr Radius Resolution Using DNA Origami. *Nature Nanotechnology* **2015**, *11* (1), 47–52. https://doi.org/10.1038/nnano.2015.240.

(45) Fu, X.; Peng, F.; Lee, J.; Yang, Q.; Zhang, F.; Xiong, M.; Kong, G.; Meng, H.; Ke, G.; Zhang, X.-B. Aptamer-Functionalized DNA Nanostructures for Biological Applications. *Topics in Current Chemistry* **2020**, *378* (2), 21. https://doi.org/10.1007/s41061-020-0283-y.

(46) Xiao, M.; Lai, W.; Man, T.; Chang, B.; Li, L.; Chandrasekaran, A. R.; Pei, H. Rationally Engineered Nucleic Acid Architectures for Biosensing Applications. *Chemical Reviews* **2019**, *119* (22), 11631–11717. https://doi.org/10.1021/ACS.CHEMREV.9B00121.

(47) Sprengel, A.; Lill, P.; Stegemann, P.; Bravo-Rodriguez, K.; Schöneweiß, E. C.; Merdanovic, M.; Gudnason, D.; Aznauryan, M.; Gamrad, L.; Barcikowski, S.; Sanchez-Garcia, E.; Birkedal, V.; Gatsogiannis, C.; Ehrmann, M.; Saccà, B. Tailored Protein Encapsulation into a DNA Host Using Geometrically Organized Supramolecular Interactions. *Nature Communications 2017 8:1* **2017**, *8* (1), 1–12. https://doi.org/10.1038/ncomms14472.

(48) Ranallo, S.; Porchetta, A.; Ricci, F. DNA-Based Scaffolds for Sensing Applications. *Analytical Chemistry* **2019**, *91* (1), 44–59. https://doi.org/10.1021/ACS.ANALCHEM.8B05009.

(49) Aghebat Rafat, A.; Sagredo, S.; Thalhammer, M.; Simmel, F. C. Barcoded DNA Origami Structures for Multiplexed Optimization and Enrichment of DNA-Based Protein-Binding Cavities. *Nature Chemistry* **2020**, *12* (9), 852–859. https://doi.org/10.1038/s41557-020-0504-6.

(50) Mela, I.; Vallejo-Ramirez, P. P.; Makarchuk, S.; Christie, G.; Bailey, D.; Henderson, R. M.; Sugiyama, H.; Endo, M.; Kaminski, C. F. DNA Nanostructures for Targeted Antimicrobial Delivery. *Angewandte Chemie* **2020**, *132* (31), 12798–12802. https://doi.org/10.1002/ANGE.202002740.

(51) Nan, Y. Focused Ion Beam Systems: Basics and Applications. *Focused Ion Beam Systems: Basics and Applications* **2007**, *9780521831994*, 1–391. https://doi.org/10.1017/CBO9780511600302.

(52) Freeley, M.; Worthy, H. L.; Ahmed, R.; Bowen, B.; Watkins, D.; Macdonald, J. E.; Zheng, M.; Jones, D. D.; Palma, M. Site-Specific One-to-One Click Coupling of Single Proteins to

Individual Carbon Nanotubes: A Single-Molecule Approach. *J Am Chem Soc* **2017**, *139* (49), 17834–17840. https://doi.org/10.1021/JACS.7B07362.

(53) Reddington, S. C.; Tippmann, E. M.; Jones, D. D. Residue Choice Defines Efficiency and Influence of Bioorthogonal Protein Modification via Genetically Encoded Strain Promoted Click Chemistry. *Chemical Communications* **2012**, *48* (67), 8419–8421. https://doi.org/10.1039/C2CC31887C.

(54) Huang, D. DNA Nanotechnology and Nanopatterning : Biochips for Single-Molecule Investigations Research Degree Thesis. **2017**.

(55) Freeley, M.; Gwyther, R. E. A.; Jones, D. D.; Palma, M. DNA-Directed Assembly of Carbon Nanotube–Protein Hybrids. *Biomolecules* **2021**, *11* (7), 955. https://doi.org/10.3390/BIOM11070955.

(56) Green, C. M.; Hughes, W. L.; Graugnard, E.; Kuang, W. Correlative Super-Resolution and Atomic Force Microscopy of DNA Nanostructures and Characterization of Addressable Site Defects. *ACS Nano* **2021**, *15* (7), 11597–11606. https://doi.org/10.1021/ACSNANO.1C01976.

(57) Martin, J. A.; Chávez, J. L.; Chushak, Y.; Chapleau, R. R.; Hagen, J.; Kelley-Loughnane, N. Tunable Stringency Aptamer Selection and Gold Nanoparticle Assay for Detection of Cortisol. *Analytical and Bioanalytical Chemistry* **2014**, *406* (19), 4637–4647. https://doi.org/10.1007/S00216-014-7883-8.

(58) The ATTO 488 Was Attached to a DNA Aptamer Relevant to Cortisol Sensing (Called Dye-Labeled SsDNA). As the Sequences of the Dye-Labeled SsDNA Tended to Self-Dimerize, the Capturing SsDNA in the DNA Origami Was Designed to Hybridise to the Dye-Labeled SsDNA in Such a Way That a Single Dye-Labeled SsDNA Was Placed on the Face of the Origami.

(59) Other Subpopulations Included Single Step Transitions from High to Low (Background) to High (1.6%), High-Low-High-Low (1.6%), Low-High (1.6%), and Low-High-Low (6.3%).

(60) Garcia-Parajo, M. F.; Segers-Nolten, G. M. J.; Veerman, J. A.; Greve, J.; van Hulst, N. F. Real-Time Light-Driven Dynamics of the Fluorescence Emission in Single Green Fluorescent Protein Molecules. *Proc Natl Acad Sci U S A* **2000**, *97* (13), 7237–7242. https://doi.org/10.1073/PNAS.97.13.7237.

(61) Dickson, R. M.; Cubittt, A. B.; Tsient, R. Y.; Moerner, W. E. On/off Blinking and Switching Behaviour of Single Molecules of Green Fluorescent Protein. *Nature* **1997**, *388* (6640), 355–358. https://doi.org/10.1038/41048.

(62) Thomas, S. K.; Jamieson, W. D.; Gwyther, R. E. A.; Bowen, B. J.; Beachey, A.; Worthy, H. L.; Macdonald, J. E.; Elliott, M.; Castell, O. K.; Jones, D. D. Site-Specific Protein Photochemical Covalent Attachment to Carbon Nanotube Side Walls and Its Electronic Impact on Single

Molecule Function. *Bioconjugate Chemistry* **2020**, *31* (3), 584–594. https://doi.org/10.1021/ACS.BIOCONJCHEM.9B00719.

(63) Plénat, T.; Yoshizawa, S.; Fourmy, D. DNA-Guided Delivery of Single Molecules into Zero-Mode Waveguides. *ACS Applied Materials and Interfaces* **2017**, *9* (36), 30561–30566. https://doi.org/10.1021/ACSAMI.7B11953.

(64) Munzar, J. D.; Ng, A.; Juncker, D. Comprehensive Profiling of the Ligand Binding Landscapes of Duplexed Aptamer Families Reveals Widespread Induced Fit. *Nature Communications* **2018**, *9* (1), 1–15. https://doi.org/10.1038/s41467-017-02556-3.

(65) Fuller, C. W.; Padayatti, P. S.; Abderrahim, H.; Adamiak, L.; Alagar, N.; Ananthapadmanabhan, N.; Baek, J.; Chinni, S.; Choi, C.; Delaney, K. J.; Dubielzig, R.; Frkanec, J.; Garcia, C.; Gardner, C.; Gebhardt, D.; Geiser, T.; Gutierrez, Z.; Hall, D. A.; Hodges, A. P.; Hou, G.; Jain, S.; Jones, T.; Lobaton, R.; Majzik, Z.; Marte, A.; Mohan, P.; II, P. M.; Mudondo, P.; Mullinix, J.; Nguyen, T.; Ollinger, F.; Orr, S.; Ouyang, Y.; Pan, P.; Park, N.; Porras, D.; Prabhu, K.; Reese, C.; Ruel, T.; Sauerbrey, T.; Sawyer, J. R.; Sinha, P.; Tu, J.; Venkatesh, A. G.; VijayKumar, S.; Zheng, L.; Jin, S.; Tour, J. M.; Church, G. M.; Mola, P. W.; Merriman, B. Molecular Electronics Sensors on a Scalable Semiconductor Chip: A Platform for Single-Molecule Measurement of Binding Kinetics and Enzyme Activity. *Proc Natl Acad Sci U S A* **2022**, *119* (5). https://doi.org/10.1073/PNAS.2112812119.

(66) Xu, X.; Bowen, B. J.; Gwyther, R. E. A.; Freeley, M.; Grigorenko, B.; Nemukhin, A. v; Eklçf-Österberg, J.; Moth-Poulsen, K.; Dafydd Jones, D.; Palma, M. Tuning Electrostatic Gating of Semiconducting Carbon Nanotubes by Controlling Protein Orientation in Biosensing Devices. *Angewandte Chemie* **2021**, *133* (37), 20346–20351. https://doi.org/10.1002/ANGE.202104044.

(67) Wilner, O. I.; Weizmann, Y.; Gill, R.; Lioubashevski, O.; Freeman, R.; Willner, I. Enzyme Cascades Activated on Topologically Programmed DNA Scaffolds. *Nature Nanotechnology* **2009**, *4* (4), 249–254. https://doi.org/10.1038/nnano.2009.50.

(68) Fu, J.; Liu, M.; Liu, Y.; Woodbury, N. W.; Yan, H. Interenzyme Substrate Diffusion for an Enzyme Cascade Organized on Spatially Addressable DNA Nanostructures. *J Am Chem Soc* **2012**, *134* (12), 5516–5519. https://doi.org/10.1021/JA300897H.

(69) Gray, C. J.; Weissenborn, M. J.; Eyers, C. E.; Flitsch, S. L. Enzymatic Reactions on Immobilised Substrates. *Chemical Society Reviews* **2013**, *42* (15), 6378–6405. https://doi.org/10.1039/C3CS60018A.

(70) Daems, D.; Rutten, I.; Bath, J.; Decrop, D.; van Gorp, H.; Ruiz, E. P.; de Feyter, S.; Turberfield, A. J.; Lammertyn, J. Controlling the Bioreceptor Spatial Distribution at the Nanoscale for Single Molecule Counting in Microwell Arrays. *ACS Sensors* **2019**, *4* (9), 2327–2335. https://doi.org/10.1021/ACSSENSORS.9B00877.

(71) Wang, W.; Yu, S.; Huang, S.; Bi, S.; Han, H.; Zhang, J. R.; Lu, Y.; Zhu, J. J. Bioapplications of DNA Nanotechnology at the Solid–Liquid Interface. *Chemical Society Reviews* **2019**, *48* (18), 4892–4920. https://doi.org/10.1039/C8CS00402A.

(72) Zhang, S.; Ai, H. wang. A General Strategy to Red-Shift Green Fluorescent Protein-Based Biosensors. *Nature Chemical Biology* **2020**, *16* (12), 1434–1439. https://doi.org/10.1038/s41589-020-0641-7.

(73) Schmied, J. J.; Gietl, A.; Holzmeister, P.; Forthmann, C.; Steinhauer, C.; Dammeyer, T.; Tinnefeld, P. Fluorescence and Super-Resolution Standards Based on DNA Origami. *Nature Methods* **2012**, *9* (12), 1133–1134. https://doi.org/10.1038/nmeth.2254.

(74) Schmied, J. J.; Raab, M.; Forthmann, C.; Pibiri, E.; Wünsch, B.; Dammeyer, T.; Tinnefeld, P. DNA Origami–Based Standards for Quantitative Fluorescence Microscopy. *Nature Protocols* **2014**, *9* (6), 1367–1391. https://doi.org/10.1038/nprot.2014.079.

(75) Zhang, Y.; Ge, C.; Zhu, C.; Salaita, K. DNA-Based Digital Tension Probes Reveal Integrin Forces during Early Cell Adhesion. *Nature Communications* **2014**, *5* (1), 1–10. https://doi.org/10.1038/ncomms6167.

(76) Amoroso, G.; Ye, Q.; Cervantes-Salguero, K.; Fernández, G.; Cecconello, A.; Palma, M. DNA-Powered Stimuli-Responsive Single-Walled Carbon Nanotube Junctions. *Chemistry of Materials* **2019**, *31* (5), 1537–1542. https://doi.org/https://doi.org/10.1021/acs.chemmater.8b04483.

(77) Cervantes-Salguero, K.; Kawamata, I.; Nomura, S. I. M.; Murata, S. Unzipping and Shearing DNA with Electrophoresed Nanoparticles in Hydrogels. *Physical Chemistry Chemical Physics* **2017**, *19* (21), 13414–13418. https://doi.org/10.1039/C7CP02214J.

(78) Daljit Singh, J. K.; Luu, M. T.; Abbas, A.; Wickham, S. F. J. Switchable DNA-Origami Nanostructures That Respond to Their Environment and Their Applications. *Biophysical Reviews* **2018**, *10* (5), 1283–1293. https://doi.org/10.1007/S12551-018-0462-Z.

(79) Wang, P.; Huh, J. H.; Park, H.; Yang, D.; Zhang, Y.; Zhang, Y.; Lee, J.; Lee, S.; Ke, Y. DNA Origami Guided Self-Assembly of Plasmonic Polymers with Robust Long-Range Plasmonic Resonance. *Nano Letters* **2020**, *20* (12), 8926–8932. https://doi.org/10.1021/ACS.NANOLETT.0C04055.

(80) Mass, O. A.; Wilson, C. K.; Roy, S. K.; Barclay, M. S.; Patten, L. K.; Terpetschnig, E. A.; Lee, J.; Pensack, R. D.; Yurke, B.; Knowlton, W. B. Exciton Delocalization in Indolenine Squaraine Aggregates Templated by DNA Holliday Junction Scaffolds. *Journal of Physical Chemistry B* **2020**, *124* (43), 9636–9647. https://doi.org/10.1021/ACS.JPCB.0C06480.

(81) Qian, L.; Winfree, E.; Bruck, J. Neural Network Computation with DNA Strand Displacement Cascades. *Nature* **2011**, *475* (7356), 368–372. https://doi.org/10.1038/nature10262.

(82) Scalise, D.; Schulman, R. Controlling Matter at the Molecular Scale with DNA Circuits. *Annu. Rev. Biomed. Eng.* **2019**, *21*, 469–493. https://doi.org/10.1146/ANNUREV-BIOENG-060418-052357.

(83) Fan, S.; Wang, D.; Cheng, J.; Liu, Y.; Luo, T.; Cui, D.; Ke, Y.; Song, J. Information Coding in a Reconfigurable DNA Origami Domino Array. *Angewandte Chemie International Edition* **2020**, *59* (31), 12991–12997. https://doi.org/10.1002/ANIE.202003823.

(84) Dickinson, G. D.; Mortuza, G. M.; Clay, W.; Piantanida, L.; Green, C. M.; Watson, C.; Hayden, E. J.; Andersen, T.; Kuang, W.; Graugnard, E.; Zadegan, R.; Hughes, W. L. An Alternative Approach to Nucleic Acid Memory. *Nature Communications* **2021**, *12* (1), 1–10. https://doi.org/10.1038/s41467-021-22277-y.